Digital Discovery



PAPER

View Article Online
View Journal | View Issue



Cite this: Digital Discovery, 2024, 3, 1421

Predicting melting temperatures across the periodic table with machine learning atomistic potentials†

Christopher M. Andolina Da and Wissam A. Saidi **D**ab

Understanding how materials melt is crucial for their practical applications and development, thereby enabling us to predict their behavior in real-world environmental conditions. Accurate computation of melting temperatures (T_m) has been a long-standing pursuit involving various methods for classical potentials and first-principles calculations. However, finding literature $T_{\rm m}$ references for many elements using a clearly defined set of calculation parameters is rare. Herein we apply deep neural network atomistic potentials (DNPs), trained on density functional theory (DFT) generated datasets, to describe the melting temperature of 20 single-element materials across the Periodic Table using large-scale molecular dynamics simulations. Our results demonstrate high-fidelity with experimental observations and also with calculated reference melting temperatures, yielding an average deviation of less than 18%. We propose a straightforward elemental-group-specific relationship between $T_{\rm m}$ and cohesive energy for these calculated references to provide reliable DFT specific reference points, which we believe can be readily applied to many materials. Additionally, we compare DNP predictions for three representative elements at external pressures up to 30 GPa in molecular dynamics simulations, revealing reasonable consistency with experimental and DFT literature references despite the lack of explicit training at these high pressures. This work further extends our flexible approach to developing and modifying DNPs to create unique atomistic potentials tailored to describe atomically complex materials under extreme environmental conditions.

Received 6th March 2024 Accepted 11th June 2024

DOI: 10.1039/d4dd00069b

rsc.li/digitaldiscovery

Introduction

Accurate predictions of a material's melting provide insight into the behavior of materials under real-world and extreme conditions¹⁻⁴ and can facilitate the discovery of new materials with desirable properties. The melting temperature $(T_{\rm m})$ is a critical material parameter in variety of research fields, such as materials science,⁵⁻⁷ metallurgy,⁸⁻¹⁰ solid-state physics,¹¹⁻¹⁵ and astro/geophysics.^{3,4} The determination of $T_{\rm m}$ can be both experimentally and computationally challenging.¹⁶ For materials with large $T_{\rm m}$ (>2000 K) and/or at high pressures (>10 GPa), experimental data are rare due to experimental limitations. Computational $T_{\rm m}$ prediction has been demonstrated using various approaches (*e.g.*, hysteresis,¹⁷⁻¹⁹ two-phase coexistence,^{20,21} interface pinning,^{22,23} and other methods²⁴⁻²⁸) and has

Machine learning-based atomistic potentials (MLP),³⁸ such as deep neural network potentials (DNPs),³⁸⁻⁴¹ have emerged as promising tools to accelerate molecular dynamics (MD) simulations. These MLPs can provide accurate predictions of various material properties at a much lower computational cost than first-principles methods while providing high-fidelity simulations akin to first-principles calculations.⁴²⁻⁴⁵ Recent methodologies using MLPs, such as moment tensor potentials⁴⁶ and graph neural networks³⁷ have been demonstrated to improve material properties predictions at elevated temperatures, thus highlighting the community's need for accurate, fast, and flexible approaches to calculating these related figures of merit.

Herein, we describe the training of individual element DNPs for predicting $T_{\rm m}$ for twenty elements across the Periodic Table using molecular dynamics (MD) simulations at finite pressure.

been actively explored for decades. $^{24,25,29-36}$ The two-phase coexistence (TPC) approach employing large supercells (>10 000 atoms) is considered the "gold standard" for predicting $T_{\rm m}$, as this approach relies on very few assumptions. 37 However, accurate computational predictions based on first-principles methods, which are accurate and generally predictive, are prohibitively computationally expensive as ensuing calculations are "large" in two domains: the number of atoms in the simulation cell and the length of simulation time. 3,29

^aDepartment of Mechanical Engineering and Materials Science, University of Pittsburgh, Pittsburgh, PA 15261, USA

^bNational Energy Technology Laboratory, United States Department of Energy, Pittsburgh, PA 15236, USA

[†] Electronic supplementary information (ESI) available: Details for all DNP and DFT values for each element in the plots. As well as configuration counts and tables of reference experimental, DFT and DNP comparisons. DFT training data, DNPs, and example validation scripts. See DOI: https://doi.org/10.1039/d4dd00069b

Digital Discovery Paper

For limited systems where data is available, we compare our results with those obtained using traditional methods, such as MD simulations, DFT calculations, and experimental observations. Although some of these MLP approaches depend on extensive training datasets, in this work, we focus our training protocol on limiting the size of the datasets while we evaluate these DNPs using a MD methodology (TPC simulations) known to have a low bias of $T_{\rm m}$ predictions when used with classical atomistic potentials.

Our study demonstrates the effectiveness of MLPs in predicting T_m yielding accurate values compared to experiments based on simulations using MD simulations executed containing ~20 000 atoms, despite the datasets being trained with a relatively small supercells (<64 atoms). These findings strongly suggest the general applicability of DNPs for studying material properties of a large variety of elements, paving the way for future investigations into the behavior of complex materials under extreme conditions. This work aims to provide a pathway to generate DNP models capable of accurately modeling the melting behavior of materials. Further, this work highlights the value of DNPs as a powerful tool for discovering, designing, and characterizing materials.47-52

Computational methods

2.1 General

The training and validation of the initial DNP training datasets are described in detail elsewhere.51,53 We used the LAMMPS54 code with DeePMD-kit(v2.2.1)41 and DeepPOT-SE55 to train DNPs and predict melting temperatures using a simple twophase coexistence approach.21 We studied twenty elemental systems in this work; we used a supercell of $14 \times 14 \times 28$ to ensure our prediction of the $T_{\rm m}$ had negligible finite-size effects and a minimal impact of thermal fluctuations. The initial conventional unit cells for each element's groundstate lattice (bcc, diamond cubic, fcc, hcp, orthorhombic, or rhombohedral) configuration were taken from "The Materials Project" database⁵⁶ (Table S1†).

2.2 Training via adaptive learning

We used an adaptive learning approach to improve the previously reported $T_{\rm m}$ prediction of the initial DNPs, increasing the total configurations <1000 structures during training (Table S2†). An ensemble approach was used to identify new structures to add to these datasets using three randomly seeded DNPs and a NPT ensemble for one hundred ps with one fs timestep. We initially applied two distinct training loops for this work (Fig. 1). The first loop focused on selecting liquid phase structures at temperatures 1.0, 1.2, and 1.4 of each element's bulk experimental melting temperature $(T_{\rm m, exp})$ (Table S1†). Only up to five configurations with the largest deviations within a force tolerance of 0.3-1.5 eV Å⁻¹ were selected for generating MD trajectories with VASP.57-60 We then ran NVT as implemented in VASP described in detail previously⁵³ (VASP INCAR parameters⁶¹ are provided in the ESI† on GitHub) on each identified structure at the corresponding temperatures; these structures are then

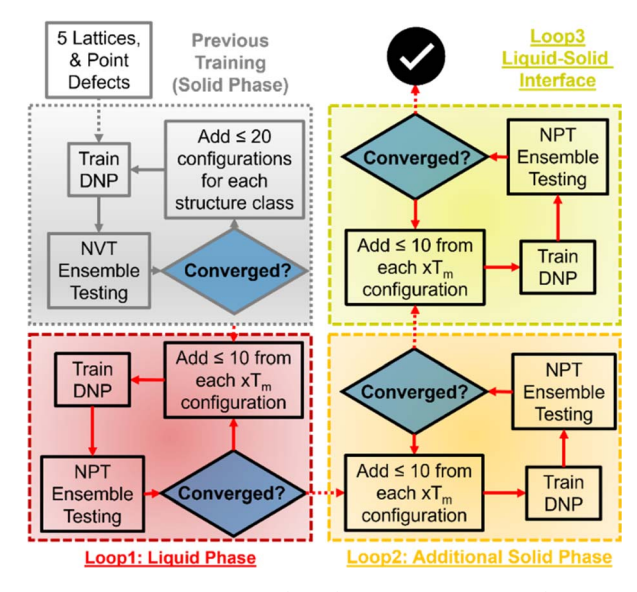


Fig. 1 Adaptive learning workflow for developing DNPs for accurate $T_{\rm m}$ predictions. The first loop adds liquid phase structures at three temperatures (xT_m ; x = 1, 1.2, and 1.4). The second loop added solid phase structures (xT_m ; x = 0.8 and 0.9), and the third loop added liquid-solid interface structures (if needed).

added to the training data to generate a new DNP. For the next iteration, we repeated this process but extended the ensemble to include structures at 0.8 and 0.9 $T_{\rm m. \, exp}$. This iterative process continued until the number of structures that matched the force criteria dwindled to less than $0.5 \text{ eV } \text{Å}^{-1}$ for all five temperatures. A final loop was run for all elements, adding solid-liquid interface structures; however, improvement of $T_{\rm m}$ predictions was only observed for Al, Os, Ti, and Zr.

Two-phase coexistence

The DNPs used were first compressed using DeePMD-kit to improve performance for these MD simulations. The simulations were run at finite external pressure, 1.0312 bar (standard atmospheric pressure) or higher for pressure-dependent testing, with an isoenthalpic ensemble (NPH) as implemented in LAMMPS with an equilibration time of one hundred twenty picoseconds (ps) at one femtosecond (fs) timestep to ensure equilibration between the solid and liquid phases. The entire simulation was first heated to melting temperature guess (for convenience, we take $T_{\rm m, guess} = T_{\rm m, exp}$) using NPT with a one hundred fs temperature and one thousand fs pressure damping frequency for ten ps. The lower half of the supercell was assigned as the liquid phase, and the upper half (along the zaxis of the crystal axis) as the solid phase. Next, the liquid phase was heated to approximately 1.25 of the $T_{\rm m,\ guess}$ for ten ps, using a NPH ensemble. The statistics for the average $T_{\rm m}$ of the simulation and standard deviation were calculated from the last twenty ps of the NPH simulation. The impact of the randomly seeded initial velocities was assessed for five distinct simulations for each elemental system with randomly seeded initial velocities. Unless noted otherwise, the errors reported are the same as those of these five simulations. Additionally, we examined the effect of the supercell using $4 \times 4 \times 8$ up to 20×10^{-2} 20×40 supercells for three representative element systems (exploring temperature range, solid phase, and atomic mass) (Li, Ni, and Re). Lastly, using the previously described methods, we explored the accuracy of three selected potentials at higher pressures up to 30 GPa in 5 GPa increments.

3. Results and discussion

The TPC MD simulation approach employed to calculate $T_{\rm m}$ excels in simplicity, i.e., no extraordinary assumptions are made. Using a mixed supercell composed of a solid and liquid phase, $T_{\rm m}$ is determined when the two phases are in equilibrium, and the melting or crystallization behavior between the phases has stabilized. Our simulations average the total system temperature over many timesteps (20 ps) to predict $T_{\rm m}$.^{29,62} We found that simulations of \sim 22 000 atoms for these calculations were an acceptable compromise of computation costs and predictive accuracy, vide infra. Starting with our previously developed elemental DNPs,53 we find that these unmodified DNPs predict $T_{\rm m}$ values with an overall modest accuracy relative to $T_{\rm m.~exp}$ at standard pressure (Fig. S1 and Table S1†) with an average percent error of 24%. We first attempted to rectify the calculated $T_{\rm m}$'s underestimation of $T_{\rm m, exp}$ by additional training through an adaptive learning approach. Indeed, we did not expect these original DNPs to describe the melting regime well as they were not trained on the elements' liquid phase, which we had expected would make the TPC calculations challenging.

Therefore, in the first iteration of adaptive learning, we added additional training structures focused on each element's liquid phase (using NPT above the experimental melting temperature at standard pressure) for all elements, see Fig. 1. We gathered results from three randomly seeded DNPs for each element, sampled 100 ps MD trajectories at 1.0, 1.2, and 1.4 multiples of the $T_{\rm m, exp,}$ and selected configurations for further training that deviated from a set force criterion 0.3 eV \mathring{A}^{-1} (Table S2†). No further training was necessary for Li, Mg, or Sr after the first adaptive learning iteration as the largest forces for new structures were <0.05 eV Å⁻¹, well below our threshold. We examined force deviations of liquid, solid, and liquid-solid interfaces for the remaining elements to improve the $T_{\rm m}$'s prediction. Finally, we re-evaluated basic material benchmark properties (Table S3†), as discussed elsewhere.53 We note improved predictive accuracy compared with DFT for cohesive energy (E_{coh}) , yielding an average error and standard deviation of <2%.

3.1 Finite-size effects on $T_{\rm m}$

Thermal fluctuations in MD simulations increase with increasing temperature and decrease with the number of atoms. Therefore, we use large supercell sizes of +10 000 or more atoms to mitigate these inherent noise sources and to improve predictive accuracy. Of course, simulations with so many atoms are highly impractical for DFT calculations due to the high computational costs that would be incurred. Nevertheless, the ease of availability for which atomistic (machine learning) potentials utilize large numbers of atoms and over long timescales (100's of ps), which DFT cannot readily achieve without great computational expense, is a significant asset similar to what has been previously demonstrated for classical potentials (e.g., embedded atom models and modified embedded atom models). This is especially valuable when the atomistic potential training is streamlined and requires less oversight from the operator, a general distinction from previous classical potential developments.

To assess finite-size effects, we investigated three elements with low (Li), moderate (Ni), and high (Nb) experimental melting temperatures (Fig. 1). Due to the stochastic nature of the MD trajectory that depends on how the simulations are initiated, our $T_{\rm m}$'s are reported as the average obtained from three randomly seeded initial temperature velocities (Table S4†) with the standard error of the mean (sem). Fig. S2† suggests that supercells with \sim 22 000 atoms (14 \times 14 \times 28, fcc conventional unit cell) are sufficiently large to reduce thermal noise to less than 5 K. We find that the employed TCP approach is sensitive to the total number of atoms of the supercell. However, it is challenging to discern if this dependency is solely a result of improving the uncertainty as the number of atoms increases or other finite-size effects, such as long-range interactions. Also, we note, unsurprisingly, that the $1/\sqrt{N}$ dependence of the sem, with the number of atoms N in the simulation (Fig. 2), is consistent with the fluctuation trends in the canonical ensemble.

To be thorough, we examined the differences in the $T_{\rm m}$ TPC-DNP results from the final DNP iteration for each element to understand the precision of the randomly seeded DNPs. We find close agreement, as expected, after one or more iterations of adaptive learning training via this stochastic approach. We emphasize the distinction of this analysis from the noise analvsis using three randomly seeded initialized velocities (vide

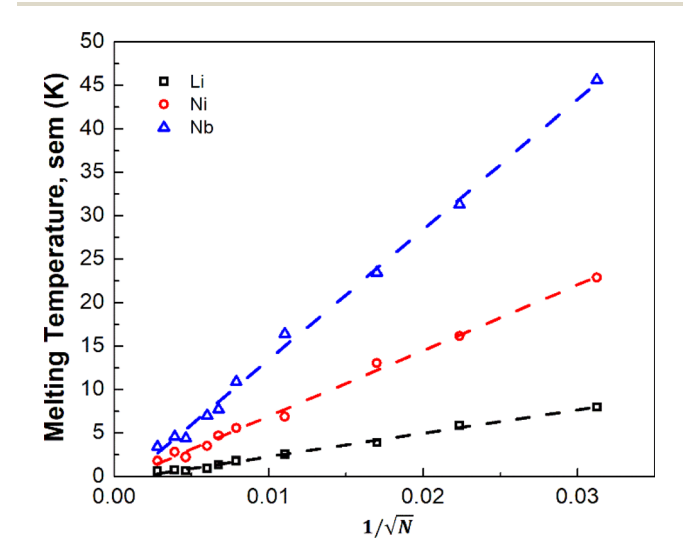


Fig. 2 The impact of supercell size N (atoms) on the thermal noise in the simulations of three randomly seeded initial velocity starting points for Li, Ni, and Nb.

supra) compared to this assessment of the DNP training/dataset using three randomly seeding DNPs. For Li, Ni, and Nb, we find that the errors are similar to what we observe from the randomly seeded DNPs (Tables S1, S4, and S5†), suggesting that the potentials are well-trained and that any intrinsic errors are inherent to the accuracies of the DFT approach. These statistical analyses provide not only an assessment of the robustness of the DNP model for MD simulations but also a reasonable estimation of the accuracy of the DNP training and dataset.

Using the simulation protocol of the TPC simulations established and validated for Li, Ni, and Nb, we computed T_{m} for all selected elements. Fig. 3A (Table S6†) summarizes the DNP as the predicted $T_{\rm m}$ increases (Re, Mo, Nb, and Os have the largest error), consistent with the expected observations of MD simulations (e.g., increasing thermal noise with increasing temperature). To ensure that finite-size effects in the training data structure for the DNP potential have no appreciable effect, we compared our results with two embedded atom models (EAM) potentials⁶³⁻⁶⁵ located in the NIST Interatomic Potential Repository. 66 We note that the finite-size impact on $T_{\rm m}$ is small for these simulation cell ranges (8 \times 8 \times 16 to 20 \times 20 \times 40) and is more evident when simulations are under $(8 \times 8 \times 16)$. Also, results obtained with the MLPs show similar trends in thermal noise reduction as those obtained with the EAM potentials. Furthermore, this comparison suggests that neither the training dataset nor the DNP model shows significant differences from classical potential behaviors (Fig. S3†) regarding finite-size effects.

3.2 DNP-TPC $T_{\rm m}$ validation

In our initial validation, we elected to compare our findings with experimental reference values over DFT-derived reference values for two reasons: (1) TPC DFT simulations in practice suffer from small supercells and large thermal fluctuations; (2) the DFT reference values in the literature could only be found

for $\frac{3}{4}$ of the investigated elements in this study, namely Ag, ⁶⁷ Al, ⁶⁸ Au, ⁶⁹ Cu, ⁷⁰ Li, ⁷¹ Mg, ⁷² Mo, ⁷³ Ni, ⁷⁴ Os, ⁷⁵ Pb, ⁷⁶ Pd, ⁷⁷ Pt, ⁷⁸ Re, ⁷⁹ Sr, ⁸⁰ and Zr⁸¹ (Table S6†). However, we cannot straightforwardly compare these studies given that they are heterogeneous in the adapted computational framework, such as in the exchange-correlation functional, pseudopotentials, DFT codes, and simulation cut-offs. Further, these calculations may be impacted by finite-size effects.

There are a handful of recent studies using DNPs to predict $T_{\rm m}$. Although the training datasets are more extensive and were developed using different approaches compared to this work, we note relatively good agreement with this literature references for Al (918 \pm 5 K), ⁸² Cu (1210 K), ⁸³ Mg (870 K), ⁸² and Ti (1886 K)⁸⁴ with our $T_{\rm m}$ values of 923 \pm 1 K (Al), 1197 \pm 1 K (Cu), 911 \pm 1 K (Mg), and 1633 \pm 13 K (Ti), respectively. Again, there are notable differences between these studies; for example, the authors of the Ti-DNP work did not use TPC but instead a metadynamics approach with smaller supercells than ours for predicting $T_{\rm m}$.84 Nevertheless, the overall agreement is compelling and supportive of robust MD modeling using DNP for various phases and elements with good agreement regardless of the dataset composition or specific training approach (e.g., DFT training set generation parameters, and DNP model training parameters, $T_{\rm m}$ calculation approach, supercell size, etc.). However, noticeable deviations from $T_{\rm m, exp}$ depend not only on the exchangecorrelation functionals^{27,28,85,86} employed in the DFT calculations but also on other variables such as DFT code, pseudopotentials, energy cut-offs, rather than the MLP model or the adaptive training approach. Therefore, an alternative $T_{\rm m}$ reference may provide a better understanding of the DNP-TPC accuracy (Fig. 3B), discussed in detail below.

We posit that the DNP underestimation of $T_{\rm m}$ compared to corresponding experimental values is an artifact propagated from the DFT datasets utilized to train the DNPs (Fig. 3A). Admittedly, it is challenging to show this conclusively, given

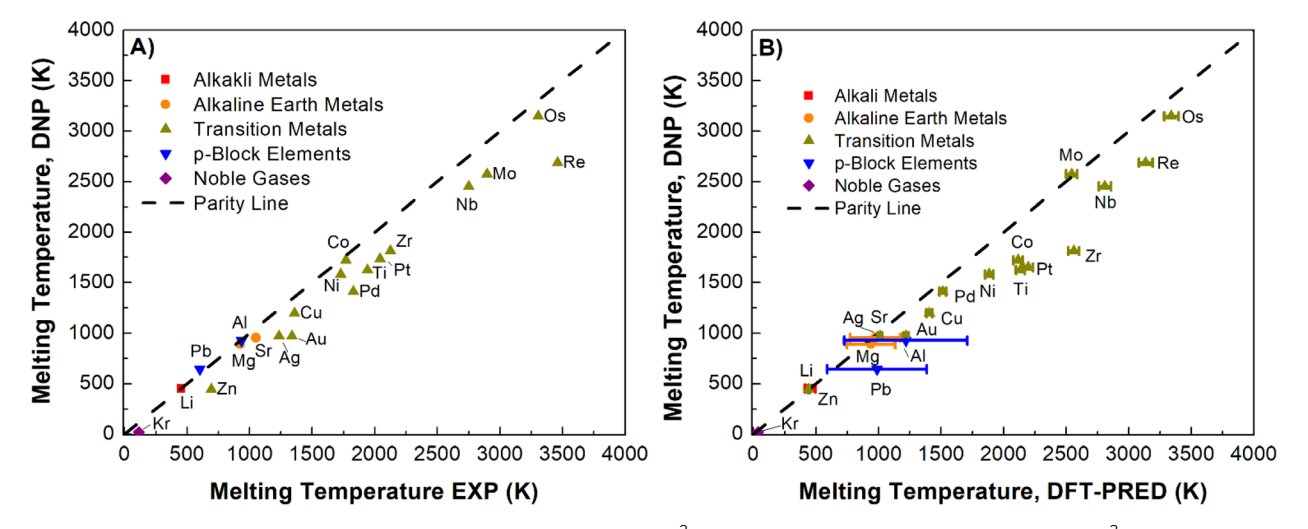


Fig. 3 Comparison of the DNP-TPC $T_{\rm m}$ versus (A) experimental results ($R^2=0.8491$) and (B) predicted DFT $T_{\rm m}$ with ($R^2=0.9896$) at standard pressure. Data on the plot are the mean of five MD simulations with randomly seeded initial velocities and the standard error of the mean, some of which are smaller than the plot symbol. In (B), y-errors bar are sems from the five simulations, and the x-errors are associated with the linear fit. The dashed line indicates the parity line.

that accurate and systematic $T_{\rm m}$ predictions are scarce using DFT with a consistent computational framework, as discussed before. However, as we argue below, this conclusion is strongly suggested, leveraging the empirical correlation between the melting temperature and the system's E_{coh} . Overall, underestimating the solid phase binding energies yields a less thermally stable solid phase; therefore, the material's melting point is predicted to occur at lower temperatures than experimentally observed.

Our study used the semi-local Perdew-Burke-Ernzerhof (PBE) functional to generate the DFT training data. Local and semi-local functionals are well-known to have shortcomings due to self-interactions that can only be rectified by accurately including the exact exchange energy, as in hybrid functionals. While PBE reproduces many experimental observables well compared to other semi-local DFT functionals,86 particularly the local-density approximation (LDA), PBE often exhibits lower bond energies. 87 This underbinding yields lower E_{coh} ; see Table S7.† For example, compared to LDA, Zhang et al. noted that PBE provides reasonable $E_{\rm coh}$ estimations for main group elements and 3d transition metals (Ti, Co, Cu, and Zn, in this work) but is less accurate for the 4d and 5d transition metals (Zr, Nb, Mo, Pd, Re, Os, Pt, and Au in this work).86 Issues from the exchangecorrelation functional could also be a concern for Zn, Ag, Au, and Pt at elevated temperatures and pressures.88

Another factor that influences the melting temperature, which is also compounded by intrinsic inaccuracies of the exchange-correlation functional, is the atomic packing of the lattice. The number of bonds or coordination number (CN) for an atom in orthorhombic, rhombohedral, diamond cubic, bcc, fcc, and hcp lattices are 2, 4, 4, 8, 12, and 12, respectively. The number of bonds in the element's solid phase is larger than the number of bonds in the liquid phase, leading to an underestimation of the propagation of the overall binding energy of the solid phase relative to the liquid phase.³⁷ These coordination numbers are significant in the context of accurate $T_{\rm m}$ predictions. The bcc (CN = 8) elements evaluated in this work (Li, Ni, and Mo) exhibit remarkable accuracy. We observe increasing average errors (relative to $T_{\rm m, exp}$) of 5, 13, and 20% for bcc (3), fcc (9), and hcp (7), respectively. This exemplifies that the transition from solid to liquid for elements with lower CN is

generally more accurate than those with more CN (e.g., fcc and hcp).89 Additionally, elements without d-electrons in their outer electron shell required minimal training (Li, Mg, and Sr), and this is consistent with the highly accurate predictions of the initial DNPs without requiring additional training.

3.3 DFT-based prediction of an element's $T_{\rm m}$

A well-known empirical relationship exists between an element's $E_{\rm coh}$ and the expected $T_{\rm m}$ value for pure metals (eqn (1)). We find a reasonable correlation ($R^2 = 0.9523$) using eqn (1) and DNP-TPC simulations (Fig. S4†). However, we expected better correlations grouping by element.

$$T_{\rm m} = 0.032 \times E_{\rm coh\text{-}EXP}/k_{\rm B} \tag{1}$$

Element group-specific linear regression was generated using alkali metals, alkaline earth metals, transition metals, pblock elements, and Noble gases, eqn (2)-(6), respectively. As shown in Fig. 4B, we find that elemental group-specific equations have appreciably better predictions for alkali metals (eqn (2), $R^2 = 0.9869$), alkaline earth metals (eqn (3), $R^2 = 0.9418$), and noble gases (eqn (6), $R^2 = 0.9992$). We also have a simple linear predictive relationship between $T_{\rm m}$ and $E_{\rm coh}$ for all dblock metals (eqn (4), Fig. S5,† $R^2 = 0.9915$). The relationship between $E_{\rm coh}$ and $T_{\rm m}$ of the p-block elements is more complex than that of the other groups discussed. We note that the reactive nonmetal group elements (C, N, O, P, S, and Se), the highly electronegative halogens (F and Cl), and post-transition metals (Ga, In, and Sn) are outliers and were not included in the p-block elements equation (eqn (5), Fig. S6,† $R^2 = 0.9176$). However, this empirical relationship fails to correlate E_{coh} and $T_{\rm m}$ for certain elements, especially the f-block elements, Fig. S7.† We also note a correlation ($R^2 = 0.9409$), Fig. S8† between $E_{\rm coh}$ (DFT) and $T_{\rm m,exp}$, but these errors are more significant than using the relationships based on experimental $T_{\rm m}$ and $E_{\rm coh}$.

$$T_{\rm m} = (0.0293 \times E_{\rm coh}/k_{\rm B}) + 430 \text{ K}$$
 (2)

$$T_{\rm m} = (0.0156 \times E_{\rm coh}/k_{\rm B}) + 162 \text{ K}$$
 (3)

$$T_{\rm m} = 0.0346 \times E_{\rm coh}/k_{\rm B} \tag{4}$$

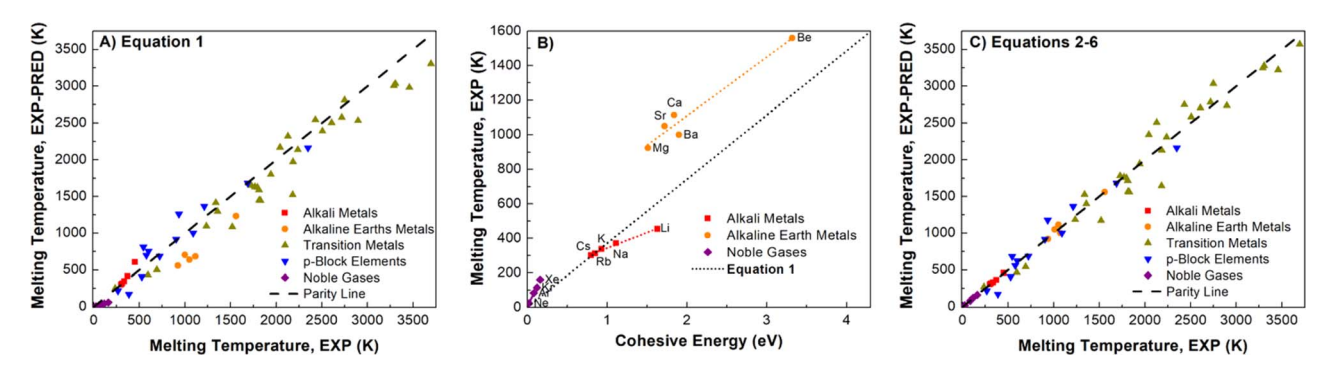


Fig. 4 Comparison of non-transition metal elements (A) parity plot showing observed $T_{m, exp}$ and predicted $T_{m, exp}$ using eqn (1) ($R^2 = 0.9857$) and (B) $T_{m, exp}$ and E_{coh} and linear fit using eqn (2), (3) and (6), the dotted line represents eqn (1). (C) $T_{m, exp}$ and $T_{m, exp}$ predicted using eqn (2)–(6) $(R^2 = 0.9914)$. Linear fits in parity plots were forced through the origin. The dashed lines are the parity lines.

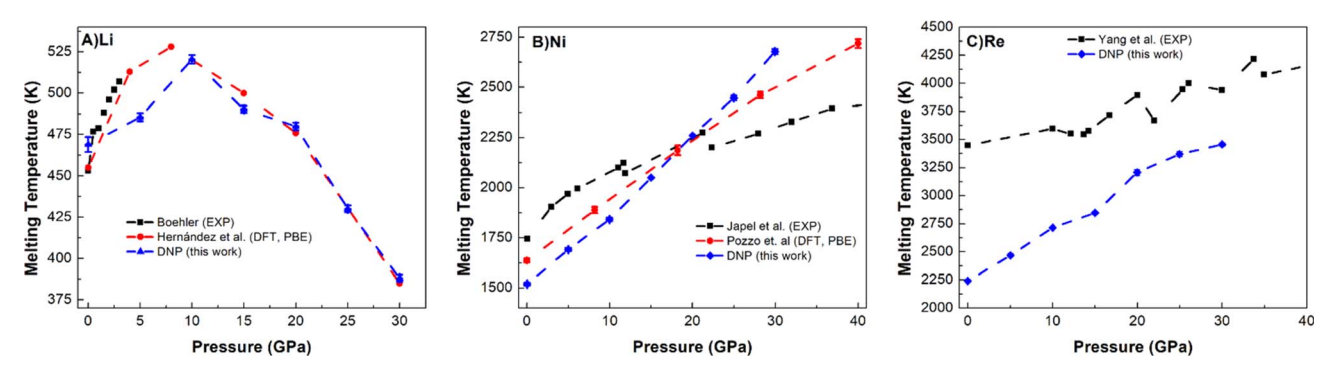


Fig. 5 Comparison of DNP TPC $T_{\rm m}$ values elevated pressures (5, 10, 15, 20, 25, and 30 GPa) with literature values for (A) Li (bcc), (B) Ni (fcc), and (C) Re (hcp). A single MD was run at each DNP point, and the 2σ was smaller than the symbol. DNP-TPC data were compared with reference literature data from first principles 71,74,91 and experiment. 89,92-94 The bars shown for Tamblyn *et al.* 91 represent $T_{\rm m}$'s calculated upper and lower bounds.

$$T_{\rm m} = (0.0351 \times E_{\rm coh}/k_{\rm B}) - 204 \text{ K}$$
 (5)

$$T_{\rm m} = (0.0873 \times E_{\rm coh}/k_{\rm B})$$
 (6)

Applying eqn (2)–(6) provides accurate predictions of $T_{\rm m,\ exp}$ (Fig. 4C). Using experimental $E_{\rm coh}$ values, we note that for this data comprised of fifty-five elements, the average % error between the $T_{\rm m,\ exp}$ and $T_{\rm m,\ exp-pred}$ decreases from 19 to 10%, respectively, for using eqn (1) and (2)–(6) (Table S8†). Extrapolating, we posit that this improvement in correlating cohesive energies and $T_{\rm m}$ also applies to the DFT values.

We had previously shown excellent agreement with DNP $E_{\rm coh}$ values for the corresponding DFT reference values, and this comparison holds even with the additional training data.⁵³

These predictions (using eqn (2)–(6)) are suitable for estimating $T_{\rm m}$ based on the DFT $E_{\rm coh}$.

3.4 Assessing the robustness of predictions at higher pressures

Lastly, we push the limits of these DNPs further by exploring the $T_{\rm m}$ predictive accuracy at high pressures (5, 10, 15, 20, 25, and 30 GPa) for select elements (Li, Ni, and Re); see Fig. 5 and Table S10.† We note that we did not explicitly train these potentials at high pressures, only at standard pressure; effectively, we are probing the extent of these DNP's functionality with these compact DFT datasets. However, the distorted lattice structures we used previously to train the initial DNPs53 have some compression, which we anticipate to be likely sufficient to describe these processes at higher pressures. Fig. 5 shows a good agreement of our melting temperature predictions as a function of pressure for these representative systems with literature values. For instance, the non-monotonic Li melting curve profile falls within the bounds of two previous DFT PBE calculations by Tamblyn et al.74 (Fig. 5A). We see an increase in $T_{\rm m}$ up to 25 GPa and 30 GPa. This anomalous negative slope from \sim 10 GPa to 30 GPa is also observed in Na and K, possibly due to the "softening" of phonon modes 95,96 and the increasing compressibility of the liquid phase.97-99 The agreement with the experimental results is reasonable;89,92 however, the DFT

predictions^{71,91} are not in agreement, and our DNP results fall between these DFT results, suggesting further research effort is needed to understand why this is observed. One explanation could be that the Li phase change from bcc to fcc at 10–30 GPa accounted for the NVT-based DFT studies, while experimental literature supports this pressure-dependent phase change at this pressure range.¹⁰⁰ We observe the fcc phase temperature and pressure regime, which are expected to occur based on experiment.¹⁰¹

The predicted $T_{\rm m}$ for Ni (Fig. 5B) and Re (Fig. 5C) follow more typical trends in $T_{\rm m}$, showing an increase in $T_{\rm m}$ as pressure increases up to 30 GPa, similar to Ni (ref. 74 and 102) and Re (ref. 93) literature values. Our predictions for Ni agree well with the DFT (PBE) calculations,74 and the agreement is reasonable with experimental observations.89 For Re, we note an agreement with the overall experimental trend for Yang et al. data, 93,103 which appears to improve as pressure increases. Interestingly, we could not find any DFT (PBE) calculations in the literature for comparison, and thus, this work may be a first glimpse of what a pressure-dependent $T_{\rm m}$ curve would show for DFT. These hightemperature and high-pressure calculations and experiments are difficult to conduct,104 exemplified by the few literature reports on $T_{\rm m}$ and pressure dependence for each method. As the pressure increases, the deviation between DNP/DFT and experiment decreases; this observation has been noted in previous DFT melting simulations for a variety of materials3,30,71,74 and is consistent with lower accuracy of first-principles modeling using PBE functionals at pressures close to zero.88

4. Conclusions

This work highlights the utility of DNPs and the advantages of using large supercells with a two-phase coexistence MD approach to predict the melting temperature of single-element materials with various properties and melting temperatures. We use adaptive learning training to systematically expand these datasets to describe melting temperatures; we demonstrate that the corresponding DNPs generated from compact DFT training sets maintain excellent predictive ability. We show that the accuracy and the thermal noise reduction of the DNP atomistic

potentials for $T_{\rm m}$ prediction are sufficient using a TPC approach when supercells are ~22 000 (14 × 14 × 28, fcc conventional unit cell). This highly flexible DNP adaptive training approach can be applied to environments outside the DFT training set with high fidelity. The DNPs' prediction of $T_{\rm m}$'s deviations from the experiment is explained in the context of the intrinsic shortcomings of the PBE functional employed in our study. However, these DNPs allow for predictions with high-fidelity to the first-principles calculations. This approach can be readily adapted to more complex materials and/or evaluated under extreme conditions such as high pressures (e.g., hundreds of GPa) starting from these or the initial DFT-based training set data

Data availability

(1) Data used to generate the main text figures are found in this publication's ESI file.† (2) Due to the large DFT training data file sizes, we have deposited all of the training data to this link (https://www.github.com/saidigroup/20-DNPs-Tm.com). In addition, example validation scripts for both LAMMPs and VASP are archived, as well as the final iterations and all three randomly seeded DNPs for each of the 20 elements discussed in this study.

Author contributions

Christopher M. Andolina: conceptualization, data curation, formal analysis, investigation, methodology, resources, software, validation, visualization, writing – original draft. Wissam A. Saidi: conceptualization, formal analysis, funding acquisition, investigation, methodology, project administration, resources, software, supervision, writing – review & editing. Both authors discussed the results and edited the manuscript.

Conflicts of interest

There are no conflicts to declare.

Acknowledgements

We are grateful to the U.S. National Science Foundation (Award No. CSSI-2003808 and CBET-2130804). Computational support was provided in part by the University of Pittsburgh Center for Research Computing through the resources provided on the H2P cluster, which is supported by NSF (Award No. OAC-2117681).

Notes and references

- 1 J. Ma, W. Li, G. Yang, S. Zheng, Y. He, X. Zhang, X. Zhang and X. Zhang, *Phys. Earth Planet. Inter.*, 2020, **309**, 106602, DOI: **10.1016/j.pepi.2020.106602**.
- 2 E. N. Akhmedov, *J. Phys. Chem. Solids*, 2018, **121**, 62–66, DOI: **10.1016/j.jpcs.2018.05.011**.
- 3 D. Alfe, *Phys. Rev. Lett.*, 2005, **94**, 235701, DOI: **10.1103/ PhysRevLett.94.235701.**

- 4 S. Pan, T. Huang, A. Vazan, Z. Liang, C. Liu, J. Wang, C. J. Pickard, H.-T. Wang, D. Xing and J. Sun, *Nat. Commun.*, 2023, **14**, 1165.
- 5 H. Lu, P. Li, Z. Cao and X. Meng, *J. Phys. Chem. C*, 2009, **113**, 7598–7602.
- 6 R. Gregorio and R. Capitao, J. Mater. Sci., 2000, 35, 299-306.
- 7 J. Zhang, B. Song, Q. Wei, D. Bourell and Y. Shi, J. Mater. Sci. Technol., 2019, 35, 270–284.
- 8 T. DebRoy, T. Mukherjee, H. L. Wei, J. W. Elmer and J. O. Milewski, *Nat. Rev. Mater.*, 2021, 6, 48–68, DOI: 10.1038/s41578-020-00236-1.
- 9 L. Murr, Addit. Manuf., 2015, 5, 40-53.
- 10 R. Fandrich, H.-B. Lüngen and C.-D. Wuppermann, *Metall. Res. Technol.*, 2008, **105**, 364–374.
- 11 G. L. Pollack, Rev. Mod. Phys., 1964, 36, 748.
- 12 S. Lou, F. Zhang, C. Fu, M. Chen, Y. Ma, G. Yin and J. Wang, Adv. Mater., 2021, 33, 2000721, DOI: 10.1002/ adma.202000721.
- 13 L. Qiu, N. Zhu, Y. Feng, E. E. Michaelides, G. Żyła, D. Jing, X. Zhang, P. M. Norris, C. N. Markides and O. Mahian, *Phys. Rep.*, 2020, 843, 1–81.
- 14 B. Lilia, R. Hennig, P. Hirschfeld, G. Profeta, A. Sanna, E. Zurek, W. E. Pickett, M. Amsler, R. Dias and M. I. Eremets, J. Phys.: Condens. Matter, 2022, 34, 183002, DOI: 10.1088/1361-648X/ac2864.
- C. Wang, K. Fu, S. P. Kammampata, D. W. McOwen,
 A. J. Samson, L. Zhang, G. T. Hitz, A. M. Nolan,
 E. D. Wachsman and Y. Mo, *Chem. Rev.*, 2020, 120, 4257–4300, DOI: 10.1021/acs.chemrev.9b00427.
- 16 G. de With, *Chem. Rev.*, 2023, **123**, 13713–13795, DOI: **10.1021/acs.chemrev.3c00489**.
- 17 L. Zheng, Q. An, Y. Xie, Z. Sun and S.-N. Luo, *J. Chem. Phys.*, 2007, 127, 164503, DOI: 10.1063/1.2790424.
- 18 S. N. Luo, A. Strachan and D. C. Swift, J. Chem. Phys., 2004, 120 24, 11640–11649, DOI: 10.1063/1.1755655.
- 19 Y. W. Tang, J. Wang and X. C. Zeng, *J. Chem. Phys.*, 2006, **124**, 236103, DOI: **10.1063/1.2206592**.
- 20 S. V. Starikov and V. V. Stegailov, *Phys. Rev. B: Condens. Matter Mater. Phys.*, 2009, **80**, 220104, DOI: **10.1103/PhysRevB.80.220104**.
- 21 J. R. Morris, C. Z. Wang, K. M. Ho and C. T. Chan, *Phys. Rev. B: Condens. Matter Mater. Phys.*, 1994, 49, 3109–3115, DOI: 10.1103/PhysRevB.49.3109.
- 22 U. R. Pedersen, F. Hummel, G. Kresse, G. Kahl and C. Dellago, *Phys. Rev. B: Condens. Matter Mater. Phys.*, 2013, 88, 094101, DOI: 10.1103/PhysRevB.88.094101.
- 23 U. R. Pedersen, J. Chem. Phys., 2013, 139, 104102, DOI: 10.1063/1.4818747.
- 24 D. Frenkel and A. J. Ladd, J. Chem. Phys., 1984, 81, 3188-
- 25 G. Grochola, J. Chem. Phys., 2004, 120, 2122-2126.
- 26 S. Alavi and D. L. Thompson, *J. Chem. Phys.*, 2005, **122**, 154704, DOI: **10.1063/1.1880932**.
- 27 L.-F. Zhu, B. Grabowski and J. Neugebauer, *Phys. Rev. B*, 2017, **96**, 224202, DOI: **10.1103/PhysRevB.96.224202**.

- 28 L.-F. Zhu, F. Körmann, A. V. Ruban, J. Neugebauer and B. Grabowski, *Phys. Rev. B*, 2020, **101**, 144108, DOI: **10.1103/PhysRevB.101.144108**.
- 29 Y. Zou, S. Xiang and C. Dai, Comput. Mater. Sci., 2020, 171, 109156, DOI: 10.1016/j.commatsci.2019.109156.
- 30 D. Alfe, M. Alfredsson, J. Brodholt, M. Gillan, M. Towler and R. Needs, *Phys. Rev. B: Condens. Matter Mater. Phys.*, 2005, 72, 014114.
- 31 Q.-J. Hong and A. Van De Walle, *Phys. Rev. B: Condens. Matter Mater. Phys.*, 2015, **92**, 020104.
- 32 F. Dorner, Z. Sukurma, C. Dellago and G. Kresse, *Phys. Rev. Lett.*, 2018, **121**, 195701, DOI: **10.1103/PhysRevLett.121.195701**.
- 33 L. Chen and V. S. Bryantsev, *Phys. Chem. Chem. Phys.*, 2017, **19**, 4114–4124, DOI: **10.1039/c6cp08403f**.
- 34 G. García, M. Atilhan and S. Aparicio, *Chem. Phys. Lett.*, 2015, **634**, 151-155.
- 35 L.-F. Zhu, J. Janssen, S. Ishibashi, F. Körmann, B. Grabowski and J. Neugebauer, *Comput. Mater. Sci.*, 2021, 187, 110065, DOI: 10.1016/j.commatsci.2020.110065.
- 36 D. E. Farache, J. C. Verduzco, Z. D. McClure, S. Desai and A. Strachan, *Comput. Mater. Sci.*, 2022, 209, 111386, DOI: 10.1016/j.commatsci.2022.111386.
- 37 Q.-J. Hong, Comput. Mater. Sci., 2022, 214, 111684, DOI: 10.1016/j.commatsci.2022.111684.
- 38 Y. Zuo, C. Chen, X. Li, Z. Deng, Y. Chen, J. Behler, G. Csányi, A. V. Shapeev, A. P. Thompson, M. A. Wood and S. P. Ong, *J. Phys. Chem. A*, 2020, 124, 731–745, DOI: 10.1021/acs.jpca.9b08723.
- 39 K. Choudhary, B. DeCost, C. Chen, A. Jain, F. Tavazza, R. Cohn, C. W. Park, A. Choudhary, A. Agrawal and S. J. Billinge, *npj Comput. Mater.*, 2022, **8**, 59.
- 40 E. Kocer, T. W. Ko and J. Behler, Annu. Rev. Phys. Chem., 2022, 73, 163–186, DOI: 10.1146/annurev-physchem-082720-034254.
- 41 H. Wang, L. Zhang, J. Han and E. Weinan, *Comput. Phys. Commun.*, 2018, 228, 178–184.
- 42 C. Cheng, Y. Yang, Y. Zhong, Y. Chen, T. Hsu and J. Yeh, *Curr. Opin. Solid State Mater. Sci.*, 2017, 21, 299.
- 43 M. Haghighatlari, J. Li, X. Guan, O. Zhang, A. Das, C. J. Stein, F. Heidar-Zadeh, M. Liu, M. Head-Gordon and L. Bertels, *Digital Discovery*, 2022, 1, 333–343, DOI: 10.1039/d2dd00008c.
- 44 J. T. Margraf, Angew. Chem., Int. Ed., 2023, 62, e202219170, DOI: 10.1002/anie.202219170.
- 45 S. Axelrod, D. Schwalbe-Koda, S. Mohapatra, J. Damewood, K. P. Greenman and R. Gómez-Bombarelli, *Acc. Mater. Res.*, 2022, 3, 343–357.
- 46 J. H. Jung, P. Srinivasan, A. Forslund and B. Grabowski, npj Comput. Mater., 2023, 9, 3, DOI: 10.1038/s41524-022-00956-8.
- 47 C. M. Andolina, M. Bon, D. Passerone and W. A. Saidi, J. Phys. Chem. C, 2021, 125, 17438–17447, DOI: 10.1021/acs.jpcc.1c04403.
- 48 C. M. Andolina, P. Williamson and W. A. Saidi, *J. Chem. Phys.*, 2020, **152**, 154701, DOI: **10.1063/5.0005347**.

- 49 C. M. Andolina, J. G. Wright, N. Das and W. A. Saidi, *Phys. Rev. Mater.*, 2021, 5, 083804, DOI: 10.1103/PhysRevMaterials.5.083804.
- 50 D. Bayerl, C. M. Andolina, S. Dwaraknath and W. A. Saidi, Digital Discovery, 2022, 1, 61–69, DOI: 10.1039/d1dd00005e.
- 51 P. Wisesa, C. M. Andolina and W. A. Saidi, *Chem. Phys. Lett.*, 2023, **14**, 468–475, DOI: **10.1021/acs.jpclett.2c03445**.
- 52 W. A. Saidi, npj Comput. Mater., 2022, 8, 86.
- 53 C. M. Andolina and W. A. Saidi, *Digital Discovery*, 2023, 2, 1070–1077, DOI: 10.1039/D3DD00046J.
- 54 S. Plimpton, *J. Comput. Phys.*, 1995, **117**, 1–19, DOI: **10.1006**/jcph.1995.1039.
- 55 L. Zhang, J. Han, H. Wang, W. A. Saidi, R. Car and E. Weinan, 2018.
- 56 A. Jain, S. P. Ong, G. Hautier, W. Chen, W. D. Richards, S. Dacek, S. Cholia, D. Gunter, D. Skinner, G. Ceder and K. A. Persson, APL Mater., 2013, 1, DOI: 10.1063/1.4812323.
- 57 G. Kresse and J. Hafner, *Phys. Rev. B: Condens. Matter Mater. Phys.*, 1993, 47, 558–561.
- 58 G. Kresse and D. Joubert, *Phys. Rev. B: Condens. Matter Mater. Phys.*, 1999, **59**, 1758–1775, DOI: **10.1103/PhysRevB.59.1758**.
- 59 G. Kresse and J. Furthmuller, *Phys. Rev. B: Condens. Matter Mater. Phys.*, 1996, 54, 11169–11186, DOI: 10.1103/physrevb.54.11169.
- 60 G. Kresse and J. Furthmuller, *Comput. Mater. Sci.*, 1996, **6**, 15–50, DOI: **10.1016/0927-0256(96)00008-0**.
- 61 General INCAR parameters for each VASP calculation: ENCUT=400 eV, KSPACING=0.24, EDIFF=1e-8, ISMEAR=1, SIGMA=0.15, only the NVT temperature was varied.
- 62 K. Dang, J. Chen, B. Rodgers and S. Fensin, *Comput. Phys. Commun.*, 2023, **286**, 108667.
- 63 X.-Y. Liu, P. P. Ohotnicky, J. B. Adams, C. L. Rohrer and R. W. Hyland, *Surf. Sci.*, 1997, 373, 357–370, DOI: 10.1016/ S0039-6028(96)01154-5.
- 64 M. I. Mendelev, D. J. Srolovitz, G. J. Ackland and S. Han, J. Mater. Res., 2005, 20, 208–218, DOI: 10.1557/JMR.2005.0024.
- 65 M. I. Mendelev, M. J. Kramer, C. A. Becker and M. Asta, Philos. Mag., 2008, 88, 1723–1750, DOI: 10.1080/ 14786430802206482.
- 66 NIST Interatomic Potentials Repository, https://www.ctcms.nist.gov/potentials, accessed 05/20/2024, 2024.
- 67 S. Baty, L. Burakovsky and D. Errandonea, *J. Phys.: Condens. Matter*, 2021, 33, 485901.
- 68 J. Bouchet, F. Bottin, G. Jomard and G. Zérah, *Phys. Rev. B: Condens. Matter Mater. Phys.*, 2009, 80, 094102, DOI: 10.1103/PhysRevB.80.094102.
- 69 G. Weck, V. Recoules, J.-A. Queyroux, F. Datchi, J. Bouchet, S. Ninet, G. Garbarino, M. Mezouar and P. Loubeyre, *Phys. Rev. B*, 2020, **101**, 014106, DOI: **10.1103/PhysRevB.101.014106**.
- 70 L. Vočadlo, D. Alfè, G. D. Price and M. J. Gillan, J. Chem. Phys., 2004, 120, 2872–2878, DOI: 10.1063/1.1640344.

- 71 E. R. Hernández, A. Rodriguez-Prieto, A. Bergara and D. Alfè, Phys. Rev. Lett., 2010, 104, 185701, DOI: 10.1103/ PhysRevLett.104.185701.
- 72 C. Cui, J. Xian, H. Liu, F. Tian, X. Gao and H. Song, J. Appl. Phys., 2022, 131, 195901, DOI: 10.1063/5.0087764.
- 73 C. Cazorla, M. Gillan, S. Taioli and D. Alfè, J. Chem. Phys., 2007, 126, 194502, DOI: 10.1063/1.2735324.
- 74 M. Pozzo and D. Alfè, Phys. Rev. B: Condens. Matter Mater. Phys., 2013, 88, 024111, DOI: 10.1103/PhysRevB.88.024111.
- 75 L. Burakovsky, N. Burakovsky and D. Preston, Phys. Rev. B: Condens. Matter Mater. Phys., 2015, 92, 174105.
- 76 T. Bryk, T. Demchuk and N. Jakse, Phys. Rev. B, 2019, 99, 014201, DOI: 10.1103/PhysRevB.99.014201.
- 77 Z.-L. Liu, J.-H. Yang, L.-C. Cai, F.-Q. Jing and D. Alfè, Phys. Rev. B: Condens. Matter Mater. Phys., 2011, 83, 144113, DOI: 10.1103/PhysRevB.83.144113.
- 78 L. Burakovsky, S. P. Chen, D. L. Preston and D. G. Sheppard, J. Phys.: Conf. Ser., 2014, 500, 162001, DOI: 10.1088/1742-6596/500/16/162001.
- 79 D. Minakov, P. Levashov and M. Paramonov, 2019.
- 80 N. Bhatt, P. Vyas and A. Jani, Philos. Mag., 2010, 90, 1599-
- 81 D. Minakov, M. Paramonov, G. Demyanov, V. Fokin and P. Levashov, Phys. Rev. B, 2022, 106, 214105.
- 82 L. Zhang, D.-Y. Lin, H. Wang, R. Car and W. E, Phys. Rev. 2019, 3, 023804. DOI: 10.1103/ Mater.. PhysRevMaterials.3.023804.
- 83 Y. Du, Z. Meng, Q. Yan, C. Wang, Y. Tian, W. Duan, S. Zhang and P. Lin, Phys. Chem. Chem. Phys., 2022, 24, 18361-18369.
- 84 T. Wen, R. Wang, L. Zhu, L. Zhang, H. Wang, D. J. Srolovitz and Z. Wu, npj Comput. Mater., 2021, 7, 206, DOI: 10.1038/ s41524-021-00661-y.
- 85 L. Schimka, R. Gaudoin, J. Klimeš, M. Marsman and G. Kresse, Phys. Rev. B: Condens. Matter Mater. Phys., 2013, 87, 214102, DOI: 10.1103/PhysRevB.87.214102.
- 86 G. Zhang, New J. Phys., 2018, 20, 063020.
- 87 J. P. Perdew, A. Ruzsinszky, G. I. Csonka, O. A. Vydrov, G. E. Scuseria, L. A. Constantin, X. Zhou and K. Burke, Phys. Rev. Lett., 2008, 100, 136406, DOI: 10.1103/ PhysRevLett.100.136406.

- 88 A. Dewaele, M. Torrent, P. Loubeyre and M. Mezouar, Phys. Rev. B: Condens. Matter Mater. Phys., 2008, 78, 104102, DOI: 10.1103/PhysRevB.78.104102.
- 89 S. Japel, B. Schwager, R. Boehler and M. Ross, Phys. Rev. Lett., 2005, 95, 167801, DOI: 10.1103/ PhysRevLett.95.167801.
- 90 F. Guinea, J. H. Rose, J. R. Smith and J. Ferrante, Appl. Phys. Lett., 1984, 44, 53-55, DOI: 10.1063/1.94549.
- 91 I. Tamblyn, J.-Y. Raty and S. A. Bonev, Phys. Rev. Lett., 2008, 101, 075703, DOI: 10.1103/PhysRevLett.101.075703.
- 92 R. Boehler, Phys. Rev. B: Condens. Matter Mater. Phys., 1983, 27, 6754.
- 93 L. Yang, A. Karandikar and R. Boehler, Rev. Sci. Instrum., 2012, 83, 063905, DOI: 10.1063/1.4730595.
- 94 A. M. J. Schaeffer, W. B. Talmadge, S. R. Temple and S. Deemyad, Phys. Rev. Lett., 2012, 109, 185702, DOI: 10.1103/PhysRevLett.109.185702.
- 95 J.-Y. Raty, E. Schwegler and S. A. Bonev, Nature, 2007, 449, 448-451, DOI: 10.1038/nature06123.
- 96 E. R. Hernández and J. Íñiguez, Phys. Rev. Lett., 2007, 98, 055501, DOI: 10.1103/PhysRevLett.98.055501.
- 97 M. Martinez-Canales and A. Bergara, J. Phys. Chem. Solids, 2008, 69, 2151-2154, DOI: 10.1016/j.jpcs.2008.03.022.
- 98 L. Koči, R. Ahuja, L. Vitos and U. Pinsook, Phys. Rev. B: Condens. Matter Mater. Phys., 2008, 77, 132101, DOI: 10.1103/PhysRevB.77.132101.
- 99 S. V. Lepeshkin, M. V. Magnitskaya and E. G. Maksimov, **JETP** Lett., 2009, 89, 586-591, DOI: S0021364009110137.
- 100 A. Lazicki, Y. Fei and R. J. Hemley, Solid State Commun., 2010, 150, 625-627, DOI: 10.1016/j.ssc.2009.12.029.
- L. Guillaume, E. Gregoryanz, O. Degtyareva, 101 C. M. I. McMahon, M. Hanfland, S. Evans, M. Guthrie, S. V. Sinogeikin and H. K. Mao, Nat. Phys., 2011, 7, 211-214, DOI: 10.1038/nphys1864.
- 102 D. Errandonea, Phys. Rev. B: Condens. Matter Mater. Phys., 2013, 87, 054108.
- 103 L. Burakovsky, N. Burakovsky, D. Preston and S. Simak, Crystals, 2018, 8, 243.
- 104 P. Wisesa, C. M. Andolina and W. A. Saidi, Chem. Phys. Lett., 2023, 14, 8741-8748, DOI: 10.1021/acs.jpclett.3c02424.